Nanoparticle lattices with bases: Fourier modal method and dipole approximation

Ilia M. Fradkin*
Skolkovo Institute of Science and Technology, Nobel Street 3, Moscow 143025, Russia
and Moscow Institute of Physics and Technology, Institutskiy pereulok 9, Moscow Region 141701, Russia

Sergey A. Dyakov and Nikolay A. Gippius
Skolkovo Institute of Science and Technology, Nobel Street 3, Moscow 143025, Russia

(Received 10 March 2020; revised 18 June 2020; accepted 19 June 2020; published 31 July 2020)

The utilization of periodic structures such as photonic crystals and metasurfaces is common for light manipulation at nanoscales. One of the most widely used computational approaches to consider them and design effective optical devices is the Fourier modal method (FMM) based on Fourier decomposition of electromagnetic fields. Nevertheless, calculating periodic structures with small inclusions is often a difficult task since they induce lots of high-$k_{\|}$ harmonics that should be taken into account. In this paper, we consider small-particle lattices with bases (complex unit cells) and construct their scattering matrices via discrete dipole approximation. Afterwards, these matrices are implemented in FMM for consideration of complicated layered structures. We show the performance of the proposed hybrid approach by its application to a lattice, which routes left and right circularly polarized incident light to guided modes propagating in opposite directions. We also demonstrate its precision by spectra comparison with finite-element method calculations. The high speed and precision of this approach enable the calculation of angle-dependent spectra with very high resolution in a reasonable time, which allows resolving narrow lines unobservable by other methods.

DOI: 10.1103/PhysRevB.102.045432

I. INTRODUCTION

Electromagnetic metasurfaces representing subwavelength patterns on a chip are considered one of the most effective and convenient tools for light manipulation on a chip. In particular, metasurfaces consisting of deep-subwavelength nanoparticles are very convenient for the design of structures with desired properties. Indeed, small nanoparticles have a dipole response, which makes it easy to understand qualitatively the nature of the physical processes occurring in these structures. At the same time, the choice of dielectric or plasmonic material, the shape of the particle adjustment, and the tuning of particle resonances give us wide opportunities in the determination of their optical properties for a demonstration of bright physical effects and their application for different purposes. Such metasurfaces have already been successfully implemented for holography [1–3], demonstration and implementation of lattice plasmon resonances [4–10], biosensors [11–13], spin-orbit coupling [14], and many other purposes.

However, small particles, especially if they are plasmonic ones, induce high gradients of electromagnetic fields. This strongly complicates their numerical consideration by the means of the Fourier modal method (FMM) [15], which is the most common and natural approach for dealing with periodic structures. The fact is that FMM, also known as rigorous coupled-wave analysis (RCWA) [16], is based on Fourier decomposition of electromagnetic fields and therefore requires us to take into account too many harmonics to describe a tiny inclusion, which makes it inefficient in this case. Several approaches partially solve this problem. Li's factorization rules help to solve the problem of concurrent jump discontinuities [17]. The adaptive spatial resolution [18,19] technique also improves the convergence rate for multiscale problems and particles with a nonrectangular shape. In some papers the finite-element method was used either for modal consideration of periodic structures [20] or in combination with Fourier-based approaches for describing layers with plasmonic inclusions [21]. However, for deep-subwavelength particles, an approach based on the consideration of the lattices in the dipole approximation [22–24] is most natural. In our recent study [23,24], we considered only simple lattices, but obviously, lattices with several particles in a cell pave the way for observation of a wide range of physical phenomena. Auxiliary variation of the relative position and orientation of particles in a cell and the lattice itself makes it possible to obtain two-dimensional (2D) crystals with diverse optical properties.

Here, we expand our approach based on the combination of discrete dipole approximation (DDA) with FMM [23,24] for the consideration of lattices with bases (several particles in a cell in our case). We introduce the concept of the generalized effective polarizability tensor for several particles in a cell. An example of the method application is demonstrated in the paper: the lattice of two nanobars acts as a polarization-controlled grating coupler, which routes normally incident

*Ilia.Fradkin@skoltech.ru

 ©2020 American Physical Society

left- and right-hand circular polarization in opposite directions.

II. LATTICE WITH BASIS

The general idea of the dipole consideration of the lattice is to substitute the real particle with an ideal point electric dipole. Its dipole moment $\mathbf{P}$ can be found by an application of the polarizability tensor $\hat{\alpha}$ of this particle to the background electric field $\mathbf{E}^{\mathrm{bg}}$ at the position of the particle:

$$\mathbf{P}_{\beta,i} = \hat{\alpha}_{\beta}\mathbf{E}^{\mathrm{bg}}_{\beta,i}. \tag{1}$$

Hereinafter, we use Latin letters i and j to enumerate the cells and Greek letters β and γ for particles in a cell. A convenient approach for the calculation of the polarizability tensor $\hat{\alpha}$ of a particle in an arbitrary environment, including one lying on the interface, was reported in [23,24]. Nevertheless, any other applicable technique might be used in this case since this problem is completely independent of all the other computations.

In turn, the background electric field is the sum of the external electric field $\mathbf{E}^0$, which would have been at the position of the particles for the structure without a lattice, and the field rescattered by all the neighboring particles in a lattice. We represent this quantity as a sum of contributions of the sublattice to which the considered particle belongs and all the other sublattices:

$$\begin{aligned}\mathbf{E}^{\mathrm{bg}}_{\beta,i} &= \mathbf{E}^0_{\beta,i} + \sum_{(\gamma,j)\neq(\beta,i)} \hat{G}(\mathbf{r}_{\beta,i},\mathbf{r}_{\gamma,j})\mathbf{P}_{\gamma,j} \\ &= \mathbf{E}^0_{\beta,i} + \sum_{j\neq i} \hat{G}(\mathbf{r}_{\beta,i},\mathbf{r}_{\beta,j})\mathbf{P}_{\beta,j} \\ &\quad + \sum_{\gamma\neq\beta}\sum_{j} \hat{G}(\mathbf{r}_{\beta,i},\mathbf{r}_{\gamma,j})\mathbf{P}_{\gamma,j},\end{aligned} \tag{2}$$

where $\hat{G}(\mathbf{r}_{\mathrm{B}},\mathbf{r}_{\mathrm{A}})$ is the dyadic Green's function defining the electric field induced at the point $\mathbf{r}_{\mathrm{B}}$ by a dipole at the coordinate $\mathbf{r}_{\mathrm{A}}$. The vector $\mathbf{r}_{\beta,i}$ indicates the position of the corresponding (β,i)th particle.

Finally, in order to obtain a closed-form expression we represent the dipole moment of a particle through the background electric field acting on it and apply Bloch's theorem to connect electric fields of different cells by the phase factor:

$$\begin{aligned}\mathbf{E}^{\mathrm{bg}}_{\beta,i} &= \mathbf{E}^0_{\beta,i} + \sum_{j\neq i} \hat{G}(\mathbf{r}_{\beta,i},\mathbf{r}_{\beta,j})e^{i\mathbf{k}_{\parallel}(\mathbf{r}_{\beta,j}-\mathbf{r}_{\beta,i})}\hat{\alpha}_{\beta}\mathbf{E}^{\mathrm{bg}}_{\beta,i} \\ &\quad + \sum_{\gamma\neq\beta}\sum_{j} \hat{G}(\mathbf{r}_{\beta,i},\mathbf{r}_{\gamma,j})e^{i\mathbf{k}_{\parallel}(\mathbf{r}_{\gamma,j}-\mathbf{r}_{\gamma,i})}\hat{\alpha}_{\gamma}\mathbf{E}^{\mathrm{bg}}_{\gamma,i},\end{aligned} \tag{3}$$

where $\hbar\mathbf{k}_{\parallel}$ is an in-plane quasimomentum defined by an external wave incident on the structure. In this way, equations on the fields in different cells separate, and their solutions are connected by the Bloch theorem. Therefore, we consider a system of equations for an arbitrary cell and omit its index in the equations below. Denoting sums in an appropriate way, we express the same equation in matrix form:

$$\begin{aligned}\text{number of particles in a cell}\left\{\begin{pmatrix}\mathbf{E}^{\mathrm{bg}}_{\beta=1}\\ \mathbf{E}^{\mathrm{bg}}_{\beta=2}\\ \vdots\end{pmatrix}\right. &= \begin{pmatrix}\mathbf{E}^0_{\beta=1}\\ \mathbf{E}^0_{\beta=2}\\ \vdots\end{pmatrix} + \begin{pmatrix}\hat{C}_{11} & \hat{C}_{12} & \vdots\\ \hat{C}_{21} & \hat{C}_{22} & \vdots\\ \cdots & \cdots & \ddots\end{pmatrix} \\ &\quad \times \begin{pmatrix}\hat{\alpha}_1 & 0 & 0\\ 0 & \hat{\alpha}_2 & 0\\ 0 & 0 & \ddots\end{pmatrix}\begin{pmatrix}\mathbf{E}^{\mathrm{bg}}_{\beta=1}\\ \mathbf{E}^{\mathrm{bg}}_{\beta=2}\\ \vdots\end{pmatrix},\end{aligned} \tag{4}$$

where

$$\hat{C}_{\beta\gamma}(\mathbf{k}_{\parallel}) = \begin{cases}\sum_{j\neq i}\hat{G}(\mathbf{r}_{\beta,i},\mathbf{r}_{\beta,j})e^{i\mathbf{k}_{\parallel}(\mathbf{r}_{\beta,j}-\mathbf{r}_{\beta,i})} & \text{for } \beta=\gamma,\\ \sum_{j}\hat{G}(\mathbf{r}_{\beta,i},\mathbf{r}_{\gamma,j})e^{i\mathbf{k}_{\parallel}(\mathbf{r}_{\gamma,j}-\mathbf{r}_{\gamma,i})} & \text{for } \beta\neq\gamma.\end{cases} \tag{5}$$

Tensors $\hat{C}_{\beta\beta}$, which stand on a diagonal, come from the simple lattices [23,24] and are well known as lattice sums [22,25] or dynamic interaction constants [26]. Details on possible approaches to their calculations in certain environments are discussed in our papers [23,24] as well. The calculation of off-diagonal tensors $\hat{C}_{\beta\gamma}$ is considered in Appendix A. Also, such expressions were considered in several papers devoted to lattices with complex unit cells [25,27,28].

Although Eq. (5) leaves open the possibility of different sublattices being located in parallel, but shifted, planes, we do not consider such cases in this paper. First of all, the presented approach is developed primarily for the most practical case of a lattice deposited onto a chip in a single stage, in which there is obviously no vertical displacement δz. However, if we consider a structure in which sublattices belong to different layers and the spacing between them is large enough (at least 50–100 nm), then its properties can be attributed by means of FMM via computation of the scattering matrix of the whole structure from matrices of each layer [29]. Such a technique remains efficient since the interaction of sublattices at such distances is mostly determined by a small number of low-$\mathbf{k}_{\parallel}$ harmonics and the dipole approximation is valid. The remaining case of small δz is also tricky enough. If there is no additional in-plane shift of sublattices, then the dipole approximation is not valid at all, and even their consideration as constituents of the same layer cannot help. At the same time, if the relative in-plane shift is large enough to make valid the dipole approximation and the lattices are not separated by any interface, then most likely, we can just neglect out-of-plane shift δz, which brings us to the considered case. Guided by these reasons, we conclude that it makes no sense to include the consideration of rare, very specific cases at the cost of complicating all the derivations.

In order to emphasize that the considered lattice is complex, we denote the analog of effective polarizability, which connects the dipole moments of the particles with corresponding electric fields acting on them, as $\hat{\aleph}$:

$$\begin{pmatrix}\mathbf{P}_{\beta=1}\\ \mathbf{P}_{\beta=2}\\ \vdots\end{pmatrix} = \hat{\aleph}\begin{pmatrix}\mathbf{E}^0_{\beta=1}\\ \mathbf{E}^0_{\beta=2}\\ \vdots\end{pmatrix}, \tag{6}$$

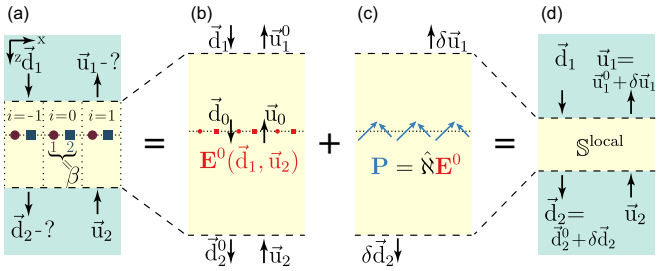

FIG. 1. Calculation of the scattering matrix of a plasmonic lattice in the dipole approximation. (a) Nanoparticle lattice in a layered medium. (b) Calculation of the external field at the position of nanoparticles (red points) in the layered medium without nanoparticles. (c) Calculation of dipole moments of nanoparticles (blue arrows). (d) Calculation of the local scattering matrix $\mathbb{S}^{\text{local}}$. In (a)–(d) dashed lines separate the local dielectric environment of the nanoparticles (yellow) from the outer dielectric environment (green). Both local and outer dielectric environments might include any number of vertically homogeneous layers and interfaces between them.

where

$$\hat{\aleph}=\begin{pmatrix}\hat{\alpha}_1 & 0 & 0\\ 0 & \hat{\alpha}_2 & 0\\ 0 & 0 & \ddots\end{pmatrix}\times\left[\hat{I}-\begin{pmatrix}\hat{C}_{11} & \hat{C}_{12} & \vdots\\ \hat{C}_{21} & \hat{C}_{22} & \vdots\\ \cdots & \cdots & \ddots\end{pmatrix}\begin{pmatrix}\hat{\alpha}_1 & 0 & 0\\ 0 & \hat{\alpha}_2 & 0\\ 0 & 0 & \ddots\end{pmatrix}\right]^{-1}. \quad (7)$$

This quantity not only enables calculation of the scattering matrix in the dipole approximation but makes the qualitative analysis of the main phenomena in such structures convenient as well. The physical sense of many effects can be understood from the structure of the matrices introduced above by analogy with Ref. [27].

III. SCATTERING MATRIX CALCULATION

The introduction of the generalized effective polarizability of the particle ensemble $\aleph$ makes it easy to calculate the dipole response of these particles on the given electric field. However, our final goal is the calculation of the scattering matrix of the so-called local layer, which contains a plasmonic lattice with its closest dielectric environment. Here we follow up on our notations and approach introduced in [23,24] and report just the required modifications for the consideration of several particles in a cell.

The basic idea reported in [23,24] is that we need to artificially insulate the local layer of the lattice from the whole structure (see Fig. 1). This layer should include the lattice itself as well as its closely disposed environment (such as an interface on which it lies) in order to get rid of high-$\mathbf{k}_\parallel$ harmonics on its boundaries. In other words, the scattering matrix of this layer will have a very limited number of elements corresponding to low-$\mathbf{k}_\parallel$ harmonics that cannot be neglected. This matrix can be represented as the sum of two terms: the first one is a scattering matrix of the background layer, which corresponds to a structure in the absence of the lattice, and the second one is obviously a contribution from this lattice:

$$\mathbb{S}^{\text{local}}=\mathbb{S}_0^{\text{local}}+\delta\mathbb{S}^{\text{local}}. \quad (8)$$

In turn, this addition can be found as

$$\delta\mathbb{S}^{\text{local}}=\mathbb{B}^{\text{out}}\mathbb{A}\mathbb{B}^{\text{in}}, \quad (9)$$

where $\mathbb{B}^{\text{in}}$ helps us to obtain the vector of amplitudes of up- and down-going waves at the plane of a lattice in the background layer from amplitudes of the incoming wave at the boundaries of this layer; the matrix $\mathbb{A}$ transfers this amplitude to discontinuities induced by currents in the lattice itself, and finally, $\mathbb{B}^{\text{out}}$ binds these discontinuities with amplitudes of outgoing waves on the boundaries of the local layer. The wonderful fact is that the expressions for $\mathbb{B}^{\text{out}}$ and $\mathbb{B}^{\text{in}}$ are exactly the same as in [23,24] for simple lattices and depend only on the structure of the background layer. $\mathbb{A}$ can be represented as an $\hat{A}$ tensor sandwiched between the material matrix of the background layer $\mathbb{F}$ and its inverse:

$$\mathbb{A}=\mathbb{F}^{-1}\hat{A}\mathbb{F}, \quad (10)$$

where $\hat{A}$ is an analog of $\mathbb{A}$ operating not with the waves' amplitudes but, rather, with field harmonics. In this way, only the matrix $\hat{A}$, which contains all the information about the lattice itself, is changed when a lattice contains more than one particle. However, its structure remains the same as for simple lattices in the original papers [23,24]. It is easy to understand that in our case the $\hat{A}$ tensor has the following form:

$$\hat{A}=\frac{-4\pi ik_0}{s}\begin{bmatrix}\hat{0} & \hat{0} & \hat{K}_x/\varepsilon\\ \hat{0} & \hat{0} & \hat{K}_y/\varepsilon\\ \hat{0} & \hat{I} & \hat{0}\\ -\hat{I} & \hat{0} & \hat{0}\end{bmatrix}\begin{bmatrix}\vec{\Gamma}_1 & \vec{0} & \vec{0}\\ \vec{0} & \vec{\Gamma}_1 & \vec{0}\\ \vec{0} & \vec{0} & \vec{\Gamma}_1\\ \vec{\Gamma}_2 & \vec{0} & \vec{0}\\ \vec{0} & \vec{\Gamma}_2 & \vec{0}\\ \vec{0} & \vec{0} & \vec{\Gamma}_2\\ \cdots & \cdots & \cdots\end{bmatrix}^{\dagger}\hat{\aleph}\times\begin{bmatrix}\vec{\Gamma}_1 & \vec{0} & \vec{0}\\ \vec{0} & \vec{\Gamma}_1 & \vec{0}\\ \vec{0} & \vec{0} & \vec{\Gamma}_1\\ \vec{\Gamma}_2 & \vec{0} & \vec{0}\\ \vec{0} & \vec{\Gamma}_2 & \vec{0}\\ \vec{0} & \vec{0} & \vec{\Gamma}_2\\ \cdots & \cdots & \cdots\end{bmatrix}\begin{bmatrix}\hat{I} & \hat{0} & \hat{0} & \hat{0}\\ \hat{0} & \hat{I} & \hat{0} & \hat{0}\\ \hat{0} & \hat{0} & \hat{K}_y/\varepsilon & -\hat{K}_x/\varepsilon\end{bmatrix}, \quad (11)$$

where s is an area of a unit cell in real space, k_0 is a wave vector in vacuum, ε is the permittivity of the homogeneous medium in which the lattice is located (the upper medium for the case of a lattice on an interface [23,24]), and the dagger denotes the Hermitian conjugate. K_x and K_y are dimensionless diagonal operators [15]:

$$\hat{K}_x=\frac{1}{k_0}\text{diag}(k_y+\vec{g}_x),\quad \hat{K}_y=\frac{1}{k_0}\text{diag}(k_y+\vec{g}_y), \quad (12)$$

where $\vec{g}_x$ and $\vec{g}_y$ are $1\times N_g$ hypervectors of x and y projections of reciprocal lattice vectors. $\vec{\Gamma}_\beta$ calculates the electric field at the position of the βth particle from the Fourier harmonics

and is set by the following expression:

$$\vec{\Gamma}_\beta = \exp[i(k_x + \vec{g}_x)x_\beta + i(k_y + \vec{g}_y)y_\beta], \tag{13}$$

where (x_β, y_β) are the coordinates of the β particle inside the unit cell in real space. In particular, $\vec{\Gamma}_\beta^\dagger$ can be considered a partial structure factor (F_{hkl} in x-ray crystallography) corresponding to the βth sublattice. We omit the second index numbering the cells since a particle in any cell can be considered with the same result.

Referring the reader to [23,24] for the detailed description of this matrix derivation, here we just describe the purpose of each multiplier from right to left. First, the amplitudes of harmonics of the x and y components of electric and magnetic fields are transformed to harmonics of all three components of electric fields. After that, we apply the inverse Fourier transform to determine the electric field at the position of the particles in a cell and obtain the dipole moment by applying the already-discussed $\aleph$. Then, in reverse order, we calculate the Fourier harmonics of dipole moments and transfer them to discontinuities in the electric and magnetic fields that they induce [30–32].

The approach considered in this paper is approximate and obviously has its limitations. As already mentioned above, dipole approximation requires particles to be much smaller than the wavelength and the distance to the nearest neighbors. The only difference in comparison with simple lattices, which were thoroughly considered in [24], is the presence of several particles in a cell, which makes the distance between closest neighbors less than the period of a structure. Fortunately, this condition is not very strict [24], in contrast to limits on the particle size. Indeed, an increase of the particle dimensions or refractive index of the environment results in the rapid growth of high-order multipole moments. This means that before large-scale calculations for relatively large particles we need to verify that in the considered frequency range the dipole approximation is valid by some independent approach. Particularly, the dipole approximation is not enough for the consideration of resonant dielectric particles, which support both electric and magnetic Mie resonances of close frequencies. However, the magnetodipole term can potentially be easily integrated into the presented approach since the corresponding Green's functions have a very similar form [22].

Our computational approach allows us to consider a lattice in the vicinity of an interface in two different ways. The first approach suggests describing the whole structure via the combination of lattice and interface scattering matrices. It is very convenient when the distance δz_{l-i} between them is relatively large. However, the decrease of δz_{l-i} means that the particles and their electromagnetic images come closer as well. At first, this leads to a slight increase in the number of required Fourier harmonics, and the first approach can still be used. Nonetheless, the further δz_{l-i} reduction leads to the distance between particles and their images no longer being larger than their size, and the dipole approximation is no longer valid, and the second approach must be used. Namely, when the lattice lies right on an interface or the distance between them is 50–100 nm, both the lattice and the interface should be considered inseparable constituents of the common local layer. This means that the interface should be taken into account during the calculation of polarizabilities $\hat{\alpha}$ and lattice sums $\hat{C}$ [24].

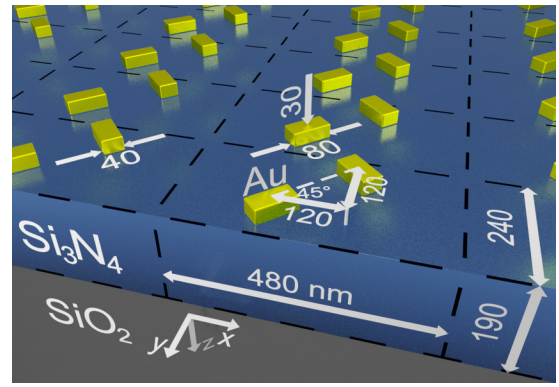

FIG. 2. Schematic of the plasmonic structure with a basis on a waveguide. All the proportions are shown in the picture in nanometers. Edges of plasmonic nanobars are smoothed out with a 1-nm-radius chamfer.

The convergence rate of our approach for simple lattices was considered in [23,24] as well. First of all, the calculation time of lattice sums $\hat{C}$ scales linearly with the number of summands, which prevents them from being a bottleneck. Nevertheless, in the case of a homogeneous environment and lattices on an interface between two homogeneous media, the diagonal blocks of lattice sums might require the computation of integrals, which, however, converge rapidly [23,24]. The calculation of off-diagonal blocks, discussed in Appendix A, is straightforward and converges asymptotically very fast, so it does not require thorough consideration. Finally, the convergence rate of the full scattering matrix, whose computational time scales cubically with the number of Fourier harmonics, does not significantly depend on the number of particles in a cell. According to [23,24], its convergence is dramatically faster in comparison to ordinary FMM, which, in turn, represents the main advantage of our method.

IV. EXAMPLE: LIGHT-ROUTING PLASMONIC METASURFACE

The ability to consider plasmonic lattices in a dipole approximation allows us to observe a large number of exciting physical phenomena. This flexibility is provided primarily by the variation of the particle's shape from symmetric disks to very elongated nanobars, their orientation, and the relative position of sublattices. In this way, the superposition of the optical properties of individual nanoparticles and the geometry of the lattice determines the behavior of guided mode excitation and, in turn, the spectra of the photonic crystals.

Here we demonstrate the performance of our approach on a lattice of two nanobars, which supports the effect often referred to as photonic spin-orbit interaction [33,34]. Our lattice is placed on a 190-nm-high Si_3N_4 ($\varepsilon_{Si_3N_4} = 4.1$) waveguide on a silica ($\varepsilon_{SiO_2} = 2.1$) substrate. Gold nanobars with a size of $80 \times 40 \times 30$ nm^3 are positioned according to Fig. 2 and are described by Johnson-Christy optical constants [35]. In order to avoid the appearance of strongly localized mesh-sensitive edge plasmons and simplify the finite-element method

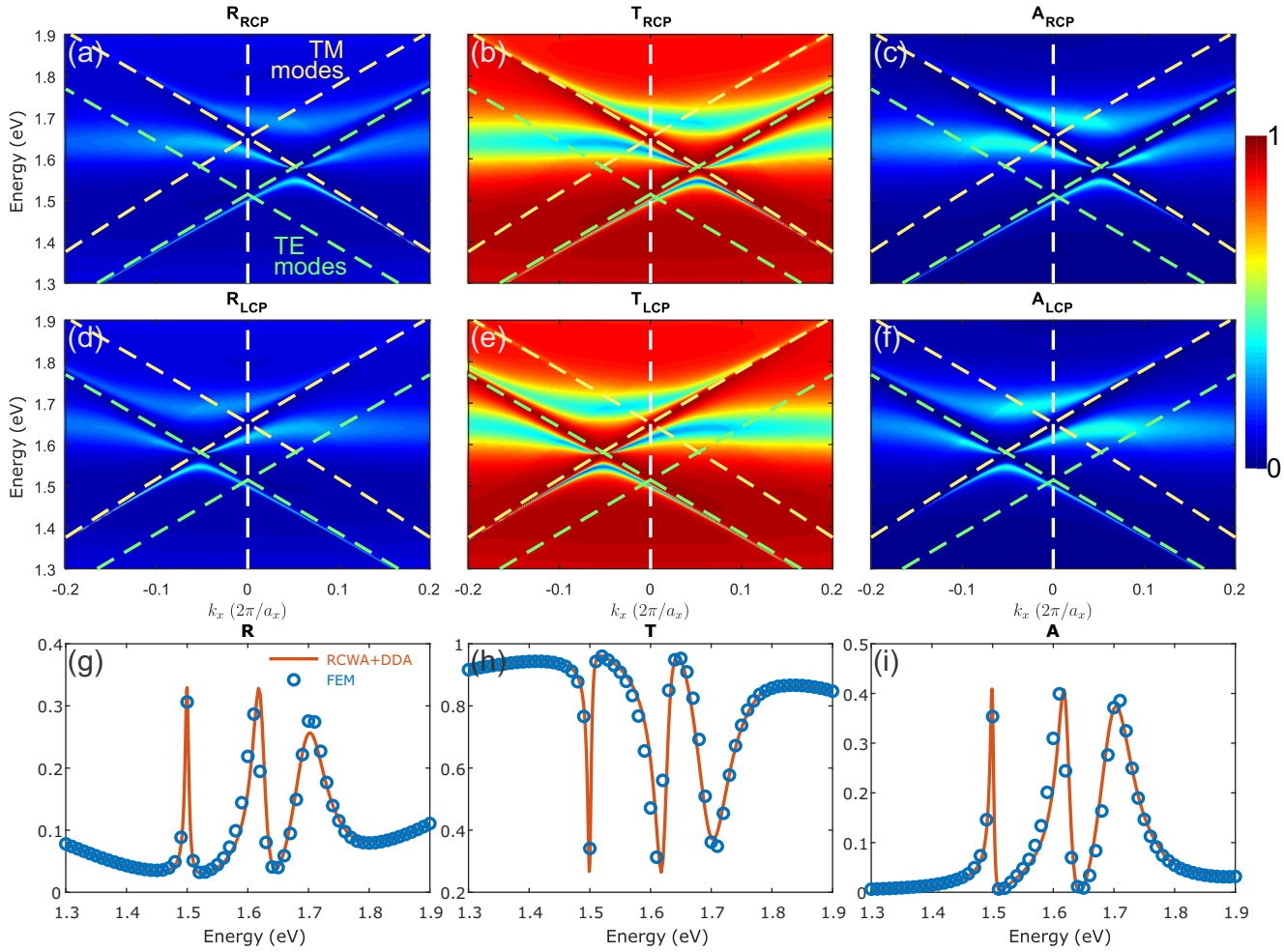

FIG. 3. In-plane wave-vector and energy dependences of (a) and (d) reflection, (b) and (e) transmission (in the main diffraction order), and (c) and (f) absorption in (a)–(c) right-handed and (d)–(f) left-handed circular polarizations for the plasmonic structure on a waveguide. Green and yellow dashed lines correspond to the TE and TM modes of a waveguide without a plasmonic lattice transferred to the first Brillouin zone. The color scale of (a)–(f) is explained on the right. (g)–(i) Spectra for the normal incidence of light, which corresponds to the $k_x = 0$ section of angle-dependent spectra. They include a comparison of computations conducted via our approach with conventional FEM calculations in COMSOL MULTIPHYSICS.

(FEM) calculation of the nanobar's polarizability tensor and reference spectra [see Figs. 3(g)–3(i)], which will be considered below, we smoothed out its edges with a 1-nm-radius smooth chamfer.

The general concept of the effect was presented in a pioneering paper [36], where the authors proposed a 2D periodic structure consisting of two sublattices of perpendicular slots in metal. Because of their perpendicularity, normally incident circularly polarized light is scattered with a $\pi/2$ phase shift by slots that belong to different sublattices. At the same time the relative shift of a quarter of the period along the x axis (as in Fig. 2) results in an additional $\pi/2$ phase shift in the excitation of guided modes (surface plasmon polariton modes in the original paper) propagating along and against the x axis. Finally, this means that sublattices excite guided modes that interfere constructively in one direction (in which phase shifts compensate each other) and destructively in the opposite one (in which phases add up and result in π shift). In other words, this structure routes light of each circular polarization to corresponding guided modes propagating in opposite directions.

Following the original idea, we illuminate the structure from above by light of both circular polarizations and observe the reflection, transmission in the main diffraction order, and absorption spectra [see Figs. 3(a)–3(f)]. Figures 3(g)–3(i) show a comparison of spectra obtained by our approach with reference points calculated by the FEM in COMSOL MULTIPHYSICS. We see that the match is very good across the whole spectrum and even the narrow lines obtained by both approaches coincide. Moreover, since the FEM is a numerical method as well and has its own finite precision, we do not even know which one is more precise. The difference between the two approaches can be considered a rough estimation of an error. However, in the case when each of the alternative approaches provides precision, which is sufficient to observe the characteristic phenomena, the issue of computation time becomes the most essential one. FEM calculations require high computational power and consume a lot of RAM. That

is why it takes about a minute to compute one point on a high-power PC. Our approach requires precomputations of the polarizability tensor, which take from several minutes to an hour in COMSOL MULTIPHYSICS depending on the required accuracy and available computational resources. However, after that, it becomes possible to obtain six spectra like those in Figs. 3(a)–3(f), each consisting of $500 \times 250 = 150\,000$ points, for any lattice from the considered particles in approximately 10 min on a regular laptop. Pictures like those in Figs. 3(g)–3(i) consisting of 300 points each are plotted in approximately 1 min.

Figures 3(a)–3(f) show that for circular polarization of an incident light k_x-dependent spectra do not have mirror symmetry with respect to the $k_x = 0$ plane. Moreover, in accordance with the symmetry of the structure all the spectra for left-hand polarized light [Figs. 3(d)–3(f)] are mirror images of corresponding right-hand circular polarization spectra [Figs. 3(a)–3(c)]. This phenomenon is clearly seen from the dispersion curves of the quasiguided modes. Indeed, the TE mode propagating to the right and the TM mode propagating to the left are excited by right-hand polarized light and vice versa for the left-hand one. Thus, we observe the desired phenomenon of spin-orbit coupling. However, in contrast to many works on surface plasmon polaritons [36–44], we have two modes of different polarizations that behave differently as well. In order to explain the considered phenomena, we build a toy model in Appendix B. Another exciting phenomenon is the strong coupling of the localized plasmonic resonance with TE and TM modes, which is observed on all the spectra. Most likely, the dipole approximation provides us with a well-known bound state in the continuum [45] in this case. However, we leave consideration of these high-quality modes for further research.

Thus, we have demonstrated that such a structure supports many interesting physical phenomena some of which can be implemented for practical purposes. First of all, this lattice can be used as a grating coupler for normally incident light toward a single mode, i.e., a single direction, in contrast to conventional ones. Second, the direction of the coupling is controlled by the polarization of light, which can be used as a convenient tool to control light propagation. Moreover, the excitation of TE and TM modes in opposite directions by a given circular polarization makes the tool set even larger. This one single example demonstrates the high diversity of possible applications that can be considered by means of the proposed approach.

V. CONCLUSION

In this paper, we have applied a calculation method combining DDA and FMM to consider periodic photonic structures with inclusions of dipole nanoparticle lattices with bases. This approach allows obtaining spectra with extremely high energy and angular resolution as it is much faster than conventional methods. Direct comparison of spectra with FEM-calculated ones demonstrated the high precision of the calculations, which makes the method reliable and applicable for practical utilization. In particular, our approach is very useful for plasmonic lattices with bases. This was demonstrated by considering a lattice supporting photonic spin-orbit coupling. This structure can be used as a circular polarization splitter for normally incident light or as a grating coupler routing TE and TM modes in opposite directions. It shows the potential of our approach for the design of practical photonic devices.

ACKNOWLEDGMENT

This work was supported by the Russian Foundation for Basic Research (Grant No. 18-29-20032).

APPENDIX A: CALCULATION OF THE GENERALIZED DYNAMIC INTERACTION CONSTANT

The concept of a generalized dynamic interaction constant for the lattice with bases is very important. However, for its practical implementation in computational approaches, we need an efficient method for its calculation. Each block of the whole tensor arising in Eq. (4) has the form defined by Eq. (5).

Since we consider dipole lattices located only in environments that are translation invariant in the x-y plane, the Green's function can be taken to be a convolution kernel. This leads to the equality of all the diagonal blocks, which correspond to the self-action of a certain sublattice since they do not depend on β:

$$\begin{aligned}\hat{C}_{\beta\beta} &= \sum_{j\neq i} \hat{G}(\mathbf{r}_{\beta,i}, \mathbf{r}_{\beta,j}) e^{i\mathbf{k}_\parallel(\mathbf{r}_{\beta,j}-\mathbf{r}_{\beta,i})} \\ &= \sum_{j\neq i} \hat{G}(\mathbf{r}_{\beta,i} - \mathbf{r}_{\beta,j}) e^{i\mathbf{k}_\parallel(\mathbf{r}_{\beta,j}-\mathbf{r}_{\beta,i})} \\ &= \sum_{j\neq i} \hat{G}(\mathbf{t}_{i-j}) e^{-i\mathbf{k}_\parallel(\mathbf{t}_{i-j})} \\ &= \sum_{j\neq 0} \hat{G}(\mathbf{t}_j) e^{-i\mathbf{k}_\parallel(\mathbf{t}_j)}, \end{aligned} \tag{A1}$$

where $\mathbf{t}_j$ is the jth translational vector of the lattice. Their calculation has already been discussed in many papers, and one of the approaches was considered in our work [23,24]. The calculation of off-diagonal blocks is much easier since the summation is held over the whole lattice without exclusions:

$$\begin{aligned}\hat{C}_{\beta\gamma}(\mathbf{k}_\parallel) &= \sum_{j} \hat{G}(\mathbf{r}_{\beta,i}, \mathbf{r}_{\gamma,j}) e^{i\mathbf{k}_\parallel(\mathbf{r}_{\gamma,j}-\mathbf{r}_{\gamma,i})} \\ &= \sum_{j} \hat{G}(\mathbf{r}_{\beta,i} - \mathbf{r}_{\gamma,j}) e^{i\mathbf{k}_\parallel(\mathbf{r}_{\gamma,j}-\mathbf{r}_{\gamma,i})} \\ &= \sum_{j} \hat{G}(\mathbf{r}_\beta - \mathbf{r}_\gamma + \mathbf{t}_j) e^{-i\mathbf{k}_\parallel\mathbf{t}_j}. \end{aligned} \tag{A2}$$

In principle, the sum above can be calculated as is; however, in real space the Green's function decays very slowly, and therefore, the convergence rate will be poor. The classical approach to cope with this problem in a homogeneous environment was formulated by Ewald [46] and was implemented in many papers [26,47–49]. Here we decided to apply another, very easy to implement method, which is applicable for a lattice placed onto an interface.

So the sum in (A2) can be expressed as a sum over the reciprocal lattice via the Poisson formula:

$$\hat{C}_{\beta\gamma}(\mathbf{k}_\parallel) = \sum_j \frac{4\pi^2}{s}\hat{M}(\mathbf{k}_\parallel + \mathbf{g}_j)e^{i(\mathbf{k}_\parallel+\mathbf{g}_j)(\mathbf{r}_\beta-\mathbf{r}_\gamma)}, \tag{A3}$$

where $\mathbf{g}_j$ is jth vector of the reciprocal lattice and $\hat{M}(\mathbf{k}_\parallel) = \frac{1}{4\pi^2}\int \hat{G}(\mathbf{r}_\parallel)e^{-i\mathbf{k}_\parallel\mathbf{r}_\parallel}d^2\mathbf{r}_\parallel$ is the dyadic Green's function in reciprocal space. Nevertheless, the new sum in reciprocal space converges slowly as well, and some components of the tensor do not converge at all. This is due to the fact that, technically, the dyadic Green's function is not an L^2-integrable function and therefore does not have a Fourier image from a mathematical point of view. However, high-$k_\parallel$ harmonics are mainly associated with a local high-gradient field in the vicinity of point dipoles. Therefore, if we exclude them with a smooth low-spatial-frequency filter $F(k_\parallel)$, then the interaction between particles will remain almost unchanged, whereas the asymptotic convergence rate can be made as fast as needed:

$$\hat{C}_{\beta\gamma}(\mathbf{k}_\parallel) \approx \sum_j \frac{4\pi^2}{s}F(|\mathbf{k}_\parallel + \mathbf{g}_j|)\hat{M}(\mathbf{k}_\parallel + \mathbf{g}_j)e^{i(\mathbf{k}_\parallel+\mathbf{g}_j)(\mathbf{r}_\beta-\mathbf{r}_\gamma)}. \tag{A4}$$

This formula can be used for practical calculations, but how does this filtering worsen the result? To figure it out, we need to return to real space. Indeed, multiplication in Fourier space is equivalent to a convolution in real space. This means that we substitute the dipole moment density defined by the delta function $\delta(\mathbf{r})$ with a source distributed in accordance with the inverse Fourier image of the filtering function $f(\mathbf{r}) = \int F(\mathbf{k}_\parallel)e^{i\mathbf{k}_\parallel\mathbf{r}_\parallel}d^2\mathbf{k}_\parallel$.

On the one hand, it is obvious that the narrower $f(\mathbf{r}_\parallel)$ is, the more precise the results are; on the other hand, we understand that in reality the dipole moment is not located at the point, and therefore, there is no reason to make the distribution area of a source much smaller than the size of a particle. At the same time, the wider a filter is in real space, the narrower it is in reciprocal space, and therefore, the faster convergence is. The calculation of Eq. (A4) is a relatively fast operation since all the summands are analytical functions, it does not include integrals or other costly operations, and, as a result, it does not limit the speed of calculations. Therefore, we recommend choosing a relatively narrow filter in real space. A reasonable half width of $f(\mathbf{r}_\parallel)$ for a wide range of problems is 10–20 nm.

The shape of the filter can be arbitrary but has to meet certain requirements. In reciprocal space $F(\mathbf{k}_\parallel)$ should be equal to unity for small wave vectors and decay to zero for high ones. This results in a fixed integral $\int f(\mathbf{r}_\parallel)d^2r = 4\pi^2$ in real space, which corresponds to the preservation of the total dipole moment ($4\pi^2$ is determined by the choice of the constant in the Fourier transform). Also, the width of the real-space filter should be much smaller than the distance to the nearest neighbor and wavelength.

For our implementation we have chosen the Gaussian filter since it provides fast decay in both real and reciprocal spaces:

$$f(\mathbf{r}_\parallel) = \frac{2\pi}{\sigma^2}e^{-\frac{r_\parallel^2}{2\sigma^2}}, \quad F(\mathbf{k}_\parallel) = e^{-\frac{\sigma^2k_\parallel^2}{2}}, \tag{A5}$$

where σ is a typical half width of the blurred dipole source in real space. Thus, off-diagonal blocks $\hat{C}_{\beta\gamma}$ can be found as follows:

$$\hat{C}_{\beta\gamma}(\mathbf{k}_\parallel) \approx \sum_j \frac{4\pi^2}{s}e^{-\frac{\sigma^2(\mathbf{k}_\parallel+\mathbf{g}_j)^2}{2}}\hat{M}(\mathbf{k}_\parallel + \mathbf{g}_j)e^{i(\mathbf{k}_\parallel+\mathbf{g}_j)(\mathbf{r}_\beta-\mathbf{r}_\gamma)}. \tag{A6}$$

APPENDIX B: DIPOLE TOY MODEL

In this Appendix, we develop a toy model based on the dipole approximation to explain qualitatively the observed effects in spectra in Fig. 3. We consider a system of equations on dipole moments analogous to Eqs. (1) and (2), but for the whole structure, including the waveguide. For practical calculations, there is no reason to include the waveguide in the consideration because of the necessity to fix its height and the material of the substrate, which can be easily varied within FMM. Also, since the bottom of the waveguide is far from the lattice, its inclusion in the consideration will not decrease the number of harmonics or increase the precision. However, here we are not going to repeat the procedure outlined in this paper and just focus on the main peculiarities of the obtained equations and their solutions. In this way, dipole moments of the particles are determined as a response to a sum of the electric field induced by external light and field rescattered by the lattice:

$$\begin{bmatrix}\mathbf{P}_1\\ \mathbf{P}_2\end{bmatrix} = \begin{bmatrix}\hat{\alpha}_1^{\mathrm{wg}} & 0\\ 0 & \hat{\alpha}_2^{\mathrm{wg}}\end{bmatrix}\left(\begin{bmatrix}\mathbf{E}_1^0\\ \mathbf{E}_2^0\end{bmatrix} + \begin{bmatrix}\mathbf{E}_1^{\mathrm{lattice}}\\ \mathbf{E}_2^{\mathrm{lattice}}\end{bmatrix}\right), \tag{B1}$$

where indices 1 and 2 correspond to particles positioned at the (0,0) and $(a_x/4, -a_y/2)$ coordinates, respectively (see Fig. 2). Polarizabilities of particles $\hat{\alpha}_{1,2}^{\mathrm{wg}}$ should be calculated for the case where they are placed on a waveguide. However, since the bottom of the waveguide is far from the particles, we can assume that $\hat{\alpha}_{1,2}^{\mathrm{wg}} = \hat{\alpha}_{1,2}$ with good precision, where the latter polarizabilities correspond to particles on an interface between two half-spaces of different media and were used in calculations in this paper. Moreover, from the numerical values of these tensors we know that for the sake of simplicity it is possible to consider particles uniaxial scatterers:

$$\hat{\alpha}_1 = \frac{\alpha}{2}\begin{bmatrix}1 & -1\\ -1 & 1\end{bmatrix}, \quad \hat{\alpha}_2 = \frac{\alpha}{2}\begin{bmatrix}1 & 1\\ 1 & 1\end{bmatrix}, \tag{B2}$$

where α is their polarizability along the 80-nm-long side.

Here we consider the illumination of the structure by normally incident light with energy close to either TE or TM mode excitation, which corresponds to intersections of the white dotted line with the green and yellow ones in Fig. 3. Under the resonant condition the contribution of the lattice to the background electric field acting on the particles in the considered cell can be expressed as a sum of fields of two modes propagating in opposite directions:

$$\begin{bmatrix}\mathbf{E}_1^{\mathrm{lattice}}\\ \mathbf{E}_2^{\mathrm{lattice}}\end{bmatrix} = A^{\rightarrow}\begin{bmatrix}\tilde{\mathbf{E}}_1^{\rightarrow}\\ \tilde{\mathbf{E}}_2^{\rightarrow}\end{bmatrix} + A^{\leftarrow}\begin{bmatrix}\tilde{\mathbf{E}}_1^{\leftarrow}\\ \tilde{\mathbf{E}}_2^{\leftarrow}\end{bmatrix}. \tag{B3}$$

According to the theory of quasinormal modes [50–52] and especially their application for the case of Fano resonances in periodic structures [53,54], the amplitude of each mode is proportional to the product of the particles' dipole moments and the field of a conjugate mode (propagating in the opposite

direction):

$$\begin{bmatrix} A^{\rightarrow} \\ A^{\leftarrow} \end{bmatrix} = \frac{1}{\omega - \tilde{\omega}} \frac{1}{N} \begin{bmatrix} \tilde{\mathbf{E}}_1^{\leftarrow} & \tilde{\mathbf{E}}_1^{\rightarrow} \\ \tilde{\mathbf{E}}_2^{\leftarrow} & \tilde{\mathbf{E}}_2^{\rightarrow} \end{bmatrix}^{\mathrm{T}} \begin{bmatrix} \mathbf{P}_1 \\ \mathbf{P}_2 \end{bmatrix}, \tag{B4}$$

where $\tilde{\omega}$ is the frequency of the resonant modes, which is real valued in this case, and N is the normalizing factor. Substituting Eqs. (B1) and (B3) in the latter equations (B4), we obtain the following system of equations:

$$\begin{aligned} \begin{bmatrix} A^{\rightarrow} \\ A^{\leftarrow} \end{bmatrix} = {} & \frac{1}{\omega - \tilde{\omega}} \frac{1}{N} \begin{bmatrix} \tilde{\mathbf{E}}_1^{\leftarrow} & \tilde{\mathbf{E}}_1^{\rightarrow} \\ \tilde{\mathbf{E}}_2^{\leftarrow} & \tilde{\mathbf{E}}_2^{\rightarrow} \end{bmatrix}^{\mathrm{T}} \begin{bmatrix} \hat{\alpha}_1 & 0 \\ 0 & \hat{\alpha}_2 \end{bmatrix} \begin{bmatrix} \mathbf{E}_1^0 \\ \mathbf{E}_2^0 \end{bmatrix} \\ & + \frac{1}{\omega - \tilde{\omega}} \frac{1}{N} \begin{bmatrix} \tilde{\mathbf{E}}_1^{\leftarrow} & \tilde{\mathbf{E}}_1^{\rightarrow} \\ \tilde{\mathbf{E}}_2^{\leftarrow} & \tilde{\mathbf{E}}_2^{\rightarrow} \end{bmatrix}^{\mathrm{T}} \begin{bmatrix} \hat{\alpha}_1 & 0 \\ 0 & \hat{\alpha}_2 \end{bmatrix} \\ & \times \begin{bmatrix} \tilde{\mathbf{E}}_1^{\rightarrow} & \tilde{\mathbf{E}}_1^{\leftarrow} \\ \tilde{\mathbf{E}}_2^{\rightarrow} & \tilde{\mathbf{E}}_2^{\leftarrow} \end{bmatrix} \begin{bmatrix} A^{\rightarrow} \\ A^{\leftarrow} \end{bmatrix}. \end{aligned} \tag{B5}$$

And we easily solve it:

$$\begin{aligned} \begin{bmatrix} A^{\rightarrow} \\ A^{\leftarrow} \end{bmatrix} = {} & \left((\omega - \tilde{\omega}) N \begin{bmatrix} 1 & 0 \\ 0 & 1 \end{bmatrix} \right. \\ & \left. - \begin{bmatrix} \tilde{\mathbf{E}}_1^{\leftarrow} & \tilde{\mathbf{E}}_1^{\rightarrow} \\ \tilde{\mathbf{E}}_2^{\leftarrow} & \tilde{\mathbf{E}}_2^{\rightarrow} \end{bmatrix}^{\mathrm{T}} \begin{bmatrix} \hat{\alpha}_1 & 0 \\ 0 & \hat{\alpha}_2 \end{bmatrix} \begin{bmatrix} \tilde{\mathbf{E}}_1^{\rightarrow} & \tilde{\mathbf{E}}_1^{\leftarrow} \\ \tilde{\mathbf{E}}_2^{\rightarrow} & \tilde{\mathbf{E}}_2^{\leftarrow} \end{bmatrix} \right)^{-1} \\ & \times \begin{bmatrix} \tilde{\mathbf{E}}_1^{\leftarrow} & \tilde{\mathbf{E}}_1^{\rightarrow} \\ \tilde{\mathbf{E}}_2^{\leftarrow} & \tilde{\mathbf{E}}_2^{\rightarrow} \end{bmatrix}^{\mathrm{T}} \begin{bmatrix} \hat{\alpha}_1 & 0 \\ 0 & \hat{\alpha}_2 \end{bmatrix} \begin{bmatrix} \mathbf{E}_1^0 \\ \mathbf{E}_2^0 \end{bmatrix}. \end{aligned} \tag{B6}$$

The last thing left to do is to substitute the explicit expressions for polarizabilities and the modes' fields. The case of TE mode excitation gives us

$$\tilde{\mathbf{E}}_1^{\mathrm{TE},\rightleftarrows} = \begin{bmatrix} 0 \\ 1 \end{bmatrix}, \quad \tilde{\mathbf{E}}_2^{\mathrm{TE},\rightleftarrows} = \begin{bmatrix} 0 \\ e^{\pm i \frac{2\pi}{a_x} \frac{a_x}{4}} \end{bmatrix} = \begin{bmatrix} 0 \\ \pm i \end{bmatrix}, \tag{B7}$$

which results in

$$\begin{bmatrix} A^{\mathrm{TE},\rightarrow} \\ A^{\mathrm{TE},\leftarrow} \end{bmatrix} = \frac{1/N^{\mathrm{TE}}}{\omega - \tilde{\omega}^{\mathrm{TE}} - \alpha/N^{\mathrm{TE}}} \begin{bmatrix} -1 & 1 & -i & -i \\ -1 & 1 & i & i \end{bmatrix} \begin{bmatrix} \mathbf{E}_1^0 \\ \mathbf{E}_2^0 \end{bmatrix}. \tag{B8}$$

The resonant denominator $\omega - \tilde{\omega} - \alpha/N$ corresponds to the hybridized lattice-waveguide resonance. The frequency of the hybridized resonance is equal to $\tilde{\omega}_{\mathrm{HR}} = \tilde{\omega} + \alpha/N$ and is complex because of the losses on leakage and dissipation. Since polarizabilities of particles are relatively small, this frequency is typically rather close to the frequency of the original mode of the waveguide.

Given that Right-handed circularly polarized (RCP) light normally incident on the structure induces external field $\mathbf{E}_1^{0,\mathrm{RCP}} = \mathbf{E}_2^{0,\mathrm{RCP}} \propto \frac{\sqrt{2}}{2}[\begin{smallmatrix} 1 \\ -i \end{smallmatrix}]$, we obtain

$$\begin{bmatrix} A^{\mathrm{TE},\rightarrow} \\ A^{\mathrm{TE},\leftarrow} \end{bmatrix} \propto \frac{-(1+i)\sqrt{2}}{\omega - \tilde{\omega}^{\mathrm{TE}} - \alpha/N^{\mathrm{TE}}} \frac{1}{N^{\mathrm{TE}}} \begin{bmatrix} 1 \\ 0 \end{bmatrix}. \tag{B9}$$

This means that only the TE mode propagating to the right will be excited by RCP light. Obviously, the reverse situation will be observed for Left-handed circularly polarized (LCP) light, which can excite only the left-propagating TE mode.

The same properties can be demonstrated for the TM mode. Although the TM mode has a nonzero field component along z, we consider only the field's in-plane components since they are the only ones that interact with the lattice in the framework of our model:

$$\tilde{\mathbf{E}}_1^{\mathrm{TM},\rightleftarrows} = \begin{bmatrix} 1 \\ 0 \end{bmatrix}, \quad \tilde{\mathbf{E}}_2^{\mathrm{TM},\rightleftarrows} = \begin{bmatrix} e^{\pm i \frac{2\pi}{a_x} \frac{a_x}{4}} \\ 0 \end{bmatrix} = \begin{bmatrix} \pm i \\ 0 \end{bmatrix}. \tag{B10}$$

These fields result in a very similar expression:

$$\begin{bmatrix} A^{\mathrm{TM},\rightarrow} \\ A^{\mathrm{TM},\leftarrow} \end{bmatrix} = \frac{1/N^{\mathrm{TM}}}{\omega - \tilde{\omega}^{\mathrm{TM}} - \alpha/N^{\mathrm{TM}}} \begin{bmatrix} 1 & -1 & -i & -i \\ 1 & -1 & i & i \end{bmatrix} \begin{bmatrix} \mathbf{E}_1^0 \\ \mathbf{E}_2^0 \end{bmatrix}, \tag{B11}$$

which corresponds to RCP light exciting the left-propagating TM mode and LCP light exciting the right-propagating one, which is in accordance with our calculation.

[1] G. Zheng, H. Mühlenbernd, M. Kenney, G. Li, T. Zentgraf, and S. Zhang, Nat. Nanotechnol. **10**, 308 (2015).

[2] W. Ye, F. Zeuner, X. Li, B. Reineke, S. He, C.-W. Qiu, J. Liu, Y. Wang, S. Zhang, and T. Zentgraf, Nat. Commun. **7**, 11930 (2016).

[3] Q. Wei, L. Huang, X. Li, J. Liu, and Y. Wang, Adv. Opt. Mater. **5**, 1700434 (2017).

[4] B. Auguié and W. L. Barnes, Phys. Rev. Lett. **101**, 143902 (2008).

[5] B. B. Rajeeva, L. Lin, and Y. Zheng, Nano Res. **11**, 4423 (2018).

[6] Y. Chu, E. Schonbrun, T. Yang, and K. B. Crozier, Appl. Phys. Lett. **93**, 181108 (2008).

[7] V. G. Kravets, F. Schedin, and A. N. Grigorenko, Phys. Rev. Lett. **101**, 087403 (2008).

[8] V. Kravets, A. Kabashin, W. Barnes, and A. Grigorenko, Chem. Rev. **118**, 5912 (2018).

[9] R. Guo, T. K. Hakala, and P. Törmä, Phys. Rev. B **95**, 155423 (2017).

[10] O. Reshef, M. Saad-Bin-Alam, M. J. Huttunen, G. Carlow, B. T. Sullivan, J.-M. Ménard, K. Dolgaleva, and R. W. Boyd, Nano Lett. **19**, 6429 (2019).

[11] Y. Shen, J. Zhou, T. Liu, Y. Tao, R. Jiang, M. Liu, G. Xiao, J. Zhu, Z.-K. Zhou, X. Wang, C. Jin, and J. Wang, Nat. Commun. **4**, 2381 (2013).

[12] S. R. K. Rodriguez, A. Abass, B. Maes, O. T. A. Janssen, G. Vecchi, and J. Gómez Rivas, Phys. Rev. X **1**, 021019 (2011).

[13] K. Lodewijks, W. Van Roy, G. Borghs, L. Lagae, and P. Van Dorpe, Nano Lett. **12**, 1655 (2012).

[14] Q. Jiang, J. Laverdant, C. Symonds, A. Pham, C. Leluyer, S. Guy, A. Drezet, and J. Bellessa, Phys. Rev. Appl. **10**, 014014 (2018).

[15] S. G. Tikhodeev, A. L. Yablonskii, E. A. Muljarov, N. A. Gippius, and T. Ishihara, Phys. Rev. B **66**, 045102 (2002).

[16] M. Moharam, E. B. Grann, D. A. Pommet, and T. Gaylord, J. Opt. Soc. Am. A **12**, 1068 (1995).

[17] L. Li, J. Opt. Soc. Am. A **14**, 2758 (1997).

[18] G. Granet and J.-P. Plumey, J. Opt. A **4**, S145 (2002).
[19] T. Weiss, G. Granet, N. A. Gippius, S. G. Tikhodeev, and H. Giessen, Opt. Express **17**, 8051 (2009).
[20] K. B. Dossou, L. C. Botten, A. A. Asatryan, B. C. Sturmberg, M. A. Byrne, C. G. Poulton, R. C. McPhedran, and C. M. De Sterke, J. Opt. Soc. Am. A **29**, 817 (2012).
[21] J.-P. Hugonin, M. Besbes, and P. Lalanne, Opt. Lett. **33**, 1590 (2008).
[22] Y. Chen, Y. Zhang, and A. F. Koenderink, Opt. Express **25**, 21358 (2017).
[23] I. M. Fradkin, S. A. Dyakov, and N. A. Gippius, Phys. Rev. B **99**, 075310 (2019).
[24] I. M. Fradkin, S. A. Dyakov, and N. A. Gippius, arXiv:1812.11359 (2018).
[25] A. Kwadrin and A. F. Koenderink, Phys. Rev. B **89**, 045120 (2014).
[26] P. A. Belov and C. R. Simovski, Phys. Rev. E **72**, 026615 (2005).
[27] S. Baur, S. Sanders, and A. Manjavacas, ACS Nano **12**, 1618 (2018).
[28] R. Kolkowski and A. F. Koenderink, Proc. IEEE **108**, 795 (2020).
[29] D. Y. K. Ko and J. Inkson, Phys. Rev. B **38**, 9945 (1988).
[30] H. Benisty, R. Stanley, and M. Mayer, J. Opt. Soc. Am. A **15**, 1192 (1998).
[31] S. V. Lobanov, T. Weiss, D. Dregely, H. Giessen, N. A. Gippius, and S. G. Tikhodeev, Phys. Rev. B **85**, 155137 (2012).
[32] H. Taniyama and M. Notomi, J. Appl. Phys. **103**, 083115 (2008).
[33] K. Y. Bliokh, F. J. Rodríguez-Fortuño, F. Nori, and A. V. Zayats, Nat. Photonics **9**, 796 (2015).
[34] N. Shitrit, I. Yulevich, E. Maguid, D. Ozeri, D. Veksler, V. Kleiner, and E. Hasman, Science **340**, 724 (2013).
[35] P. B. Johnson and R. W. Christy, Phys. Rev. B **6**, 4370 (1972).
[36] J. Lin, J. B. Mueller, Q. Wang, G. Yuan, N. Antoniou, X.-C. Yuan, and F. Capasso, Science **340**, 331 (2013).
[37] S.-Y. Lee, K. Kim, S.-J. Kim, H. Park, K.-Y. Kim, and B. Lee, Optica **2**, 6 (2015).
[38] X. Zhao, X. Feng, F. Liu, K. Cui, W. Zhang, and Y. Huang, ACS Photonics **7**, 212 (2020).
[39] J. B. Mueller, K. Leosson, and F. Capasso, Nano Lett. **14**, 5524 (2014).
[40] X. Yin, L. Chen, and X. Li, Opt. Express **26**, 23251 (2018).
[41] A. E. Miroshnichenko and Y. S. Kivshar, Science **340**, 283 (2013).
[42] X. Zhao, X. Feng, P. Zhao, F. Liu, K. Cui, W. Zhang, and Y. Huang, Opt. Express **27**, 22053 (2019).
[43] L. Huang, X. Chen, B. Bai, Q. Tan, G. Jin, T. Zentgraf, and S. Zhang, Light Sci. Appl. **2**, e70 (2013).
[44] F. Ding, R. Deshpande, and S. I. Bozhevolnyi, Light Sci. Appl. **7**, 17178 (2018).
[45] C. W. Hsu, B. Zhen, A. D. Stone, J. D. Joannopoulos, and M. Soljačić, Nat. Rev. Mater. **1**, 1 (2016).
[46] P. P. Ewald, Ann. Phys. (Berlin, Ger.) **369**, 253 (1921).
[47] I. Stevanovic, P. Crespo-Valero, K. Blagovic, F. Bongard, and J. R. Mosig, IEEE Trans. Microwave Theory Tech. **54**, 3688 (2006).
[48] V. G. Papanicolaou, J. Comput. Anal. Appl. **1**, 105 (1999).
[49] F. De Wette and G. Schacher, Phys. Rev. **137**, A78 (1965).
[50] P. Lalanne, W. Yan, K. Vynck, C. Sauvan, and J.-P. Hugonin, Laser Photonics Rev. **12**, 1700113 (2018).
[51] C. Sauvan, J. P. Hugonin, I. S. Maksymov, and P. Lalanne, Phys. Rev. Lett. **110**, 237401 (2013).
[52] Q. Bai, M. Perrin, C. Sauvan, J.-P. Hugonin, and P. Lalanne, Opt. Express **21**, 27371 (2013).
[53] T. Weiss, M. Mesch, M. Schäferling, H. Giessen, W. Langbein, and E. A. Muljarov, Phys. Rev. Lett. **116**, 237401 (2016).
[54] T. Weiss, M. Schäferling, H. Giessen, N. A. Gippius, S. G. Tikhodeev, W. Langbein, and E. A. Muljarov, Phys. Rev. B **96**, 045129 (2017).